Ferrofluidic torsional pendulum driven by oscillating magnetic field

Mark I. Shliomis*
Department of Mechanical Engineering, Ben-Gurion University, Beer-Sheva 84105, Israel

Michael A. Zaks†
Institute of Physics, Humboldt University of Berlin, D-12489 Berlin, Germany
(Received 15 February 2006; published 7 June 2006)

A thin disk-shaped container filled with a ferrofluid and suspended in a horizontal linearly polarized ac magnetic field can perform torsional vibrations around its vertical diameter. In contrast to a recently studied spherical pendulum, the cell is sensitive to the field direction: It exposes its edge to the stationary or slowly oscillating magnetic field, and its broad side to the field of a high frequency. When the amplitude of the latter field is increased, the state of rest gets destabilized, yielding to oscillations near the equilibrium. Further growth of the field strength results in the onset of the cell rotation. We describe sequences of local and global bifurcations which accompany those transitions.

DOI: 10.1103/PhysRevE.73.066208 PACS number(s): 05.45.−a, 75.50.Mm, 47.50.−d

I. INTRODUCTION

Let a container filled with a ferrofluid—the colloidal suspension of magnetic grains—rotate with an angular velocity $\mathbf{\Omega}$. As long as the fluid rotates as a whole, dissipation is absent. Application of an external magnetic field changes the picture. Individual magnetic moments of the particles tend to align with the field direction; this hinders the free rotation of particles. As a consequence, the angular velocity of magnetic nanoparticles $\mathbf{\Theta}$ deviates from $\mathbf{\Omega}$, and the ferrofluid rotation ceases to be rigid. Internal (nonhydrodynamical) rotation of magnetic grains relative to the surrounding liquid results in the dissipation of the kinetic energy of the fluid; this effect is viewed as the action of an internal—so-called rotational—viscosity η_R [1–9]. Originating from viscous torques acting upon magnetic grains, rotational viscosity obeys the relation $\eta_R \sim \eta\phi$, where η is the shear viscosity and $\phi \ll 1$ is the volume fraction of magnetic grains. Accordingly, η_R is much smaller than the shear viscosity. However, in the absence of shear flows (as in the case treated below), rotational viscosity is the sole source of energy dissipation and plays therefore a crucial role.

As shown in Ref. [9], the coefficient η_R is proportional to $(\Omega-\Theta)/\Omega$, therefore its value may be either positive or negative. A stationary or slowly oscillating magnetic field impedes free particle rotation $\Theta<\Omega$ thus η_R is positive. In contrast, a rapidly oscillating magnetic field forces the grains to rotate faster than the fluid does: $\Theta<\Omega$. Hence the grains spin up the fluid rotation. Such transformation of a part of the energy of the oscillating magnetic field into the kinetic energy of the fluid manifests itself as negative viscosity $\eta_R<0$ [9–15].

Recently, we described an interplay of magnetic and mechanical phenomena in a simple device: a torsional pendulum filled with a ferrofluid and driven by an oscillating magnetic field [16]. Here, dynamics is governed by the set of three coupled differential equations: the variables are the in- and off-axis components of the fluid magnetization and the angular deflection of the pendulum. When the pumping frequency strongly exceeds the pendulum eigenfrequency, this set is reduced to the sole equation of the Rayleigh type. For this limiting case, the magnetomechanical intertwinement can be interpreted in terms of rotational viscosity. Since the latter is negative, in a sufficiently strong magnetic field the "friction coefficient" in the Rayleigh-like equation becomes negative as well. As a result, the growing oscillations of the pendulum are excited; their velocity and amplitude are bounded by the negative feedback which owes to the dependence of η_R on the flow vorticity. This straightforward explanation does not help much in the situation when the pumping frequency and the pendulum eigenfrequency are of the same order. In this case, complicated temporal patterns of magnetomechanical interactions arise. According to our estimates [16], these effects can be experimentally observed at moderate amplitudes of the magnetic field.

The stated results refer to an axisymmetric pendulum: a sphere or a vertical cylinder filled with a ferrofluid and oscillating around the vertical axis of symmetry. Below we perform the analysis for a disk-shaped ferrofluid pendulum oscillating around its vertical diameter: the hollow coin-shaped cell filled with magnetic fluid and hung up by its edge. Compared to an axisymmetric one, this geometry possesses quite a few additional features.

First, the orientation of the pendulum state of rest—it can be characterized by the outward-facing normal $\mathbf{n}$ to the disk surface—is not indifferent to the direction of the external field $\boldsymbol{\mathcal{H}}$. The coin exposes its edge to the stationary or slowly oscillating magnetic field ($\mathbf{n}\perp\boldsymbol{\mathcal{H}}$), and either of its broad sides (head, tail) to the oscillatory field of a high frequency ($\mathbf{n}\parallel\boldsymbol{\mathcal{H}}$). Since the abrupt change of orientation occurs at a critical value of the product $\omega\tau$ (ω and τ being, respectively, the field frequency and the magnetization relaxation time), this effect gives a simple and reliable method for experimental measurement of τ. Further, in the sufficiently strong alternate field, the state of rest is replaced by oscillations near the equilibrium. These oscillations, caused by the

*Electronic address: shliomis@bgu.ac.il
†Electronic address: zaks@physik.hu-berlin.de

negative viscosity effect, yield in their turn to rotations of the coin-shaped container around its vertical axis. Such rotation of nonaxisymmetrical cells can be utilized for the design of efficient mixing and stirring devices driven by oscillating magnetic fields. Scenario of transition from oscillations to rotations, centered on a heteroclinic bifurcation, includes also several saddle-node bifurcations of periodic states.

The outline of the paper is as follows. In Sec. II equations of motion for the pendulum are derived, and physical mechanisms for the transition between the equilibrium states are discussed. In Sec. III the stability boundaries for these equilibria in the parameter space are determined. Analysis of weakly nonlinear states in Sec. IV discloses that the onset of the pendulum oscillations is soft for relatively low pumping frequencies, but is of the hard-mode type otherwise. Detailed description of the bifurcation diagram is presented in Sec. V, where various sequences of transitions between different states, as well, as cases of hysteresis, are discussed. In Sec. VI we summarize our findings and estimate the magnetic field, required for their experimental observation.

II. MAGNETIC TORQUE AND EQUILIBRIA

It is instructive to start with a more general case and consider an uniaxial ellipsoid filled with a ferrofluid and suspended on a soft (its elasticity is negligible) fiber in a horizontal linearly polarized magnetic field $\mathcal{H}_x=\mathcal{H}_0\cos\omega t$. If the axis of symmetry $\mathbf{n}$ of the cavity is located in the horizontal plane x-y, the ellipsoid is acted upon by the only component of *magnetic torque*:

$$\boldsymbol{\mathcal{T}}=\boldsymbol{\mathcal{M}}\times\boldsymbol{\mathcal{H}}=V\mathbf{M}\times\boldsymbol{\mathcal{H}},$$

$$\boldsymbol{\mathcal{T}}=(0,0,\mathcal{T}),\quad \mathcal{T}=-VM_y\mathcal{H}_0\cos\omega t, \tag{1}$$

where $\boldsymbol{\mathcal{M}}=\mathbf{M}V$ is the ferrofluid magnetic moment, $\mathbf{M}$ is its density (magnetization), and V is the volume of ferrofluid. Let us introduce in the x-y plane the axis x' along $\mathbf{n}$ and y' in the perpendicular direction, and use the magnetization equation [16]

$$d\mathbf{M}/dt=\boldsymbol{\Omega}\times\mathbf{M}-(\mathbf{M}-\chi\mathbf{H})/\tau,\quad \boldsymbol{\Omega}=(0,0,\dot\varphi), \tag{2}$$

where τ is the magnetization relaxation time, χ the initial magnetic susceptibility, and φ is the angular displacement of the vector $\mathbf{n}$ in the x-y plane. Then, substituting into Eq. (2) components of the internal field $H_{x'}=\mathcal{H}_{x'}-4\pi f_\parallel M_{x'}$ and $H_{y'}=\mathcal{H}_{y'}-4\pi f_\perp M_{y'}$, where $f_\parallel$ and $f_\perp$ are demagnetization factors along the axis of symmetry and in perpendicular direction, we get

$$\tau\dot M_{x'}+\kappa_\parallel M_{x'}=-\dot\varphi\tau M_{y'}+\chi\mathcal{H}_0\cos\omega t\cos\varphi,$$

$$\tau\dot M_{y'}+\kappa_\perp M_{y'}=\dot\varphi\tau M_{x'}-\chi\mathcal{H}_0\cos\omega t\sin\varphi, \tag{3}$$

where

$$\kappa_\parallel=1+4\pi\chi f_\parallel,\quad \kappa_\perp=1+4\pi\chi f_\perp. \tag{4}$$

Two time scales of the problem are periods of the driving magnetic field ω^{-1} and of the pendulum oscillations ω_0^{-1}, respectively (the latter will be evaluated below). We restrict ourselves to the case of high driving frequency $\omega\gg\omega_0$, when these time scales can be separated. On the fast time, the value of $\dot\varphi$ in Eqs. (3) can be treated as a constant. This turns Eqs. (3) into the set of *linear* equations; their integration yields

$$M_{x'}=\chi\mathcal{H}_0(a\cos\omega t+b\sin\omega t)/Z,$$

$$M_{y'}=-\chi\mathcal{H}_0(c\cos\omega t+d\sin\omega t)/Z, \tag{5}$$

with integration "constants"

$$a=-\dot\varphi\tau(\omega^2\tau^2-\kappa_\parallel\kappa_\perp-\dot\varphi^2\tau^2)\sin\varphi+[(\kappa_\parallel-\kappa_\perp)\omega^2\tau^2+\kappa_\perp(\omega^2\tau^2+\kappa_\parallel\kappa_\perp+\dot\varphi^2\tau^2)]\cos\varphi,$$

$$b=\omega\tau[\dot\varphi\tau(\kappa_\parallel+\kappa_\perp)\sin\varphi+(\omega^2\tau^2+\kappa_\perp^2-\dot\varphi^2\tau^2)\cos\varphi],$$

$$c=-[(\kappa_\parallel-\kappa_\perp)\omega^2\tau^2-\kappa_\parallel(\omega^2\tau^2+\kappa_\parallel\kappa_\perp+\dot\varphi^2\tau^2)]\sin\varphi+\dot\varphi\tau(\omega^2\tau^2-\kappa_\parallel\kappa_\perp-\dot\varphi^2\tau^2)\cos\varphi,$$

$$d=\omega\tau[(\omega^2\tau^2+\kappa_\parallel^2-\dot\varphi^2\tau^2)\sin\varphi-\dot\varphi\tau(\kappa_\parallel+\kappa_\perp)\cos\varphi],$$

$$Z=(\omega^2\tau^2-\kappa_\parallel\kappa_\perp-\dot\varphi^2\tau^2)^2+(\kappa_\parallel+\kappa_\perp)^2\omega^2\tau^2.$$

Calculating now

$$M_y=M_{x'}\sin\varphi+M_{y'}\cos\varphi=\chi\mathcal{H}_0\times[(a\sin\varphi-c\cos\varphi)\cos\omega t+(b\sin\varphi-d\cos\varphi)\sin\omega t]$$

and averaging the product $M_y\mathcal{H}_0\cos\omega t$ over the period of the field variation (i.e., over the fast time), one finds

$$\bar{\mathcal{T}}=-V\overline{M_y\mathcal{H}_0\cos\omega t}=\tfrac{1}{2}\chi\mathcal{H}_0^2V\times\frac{(\omega^2\tau^2-\kappa_\parallel\kappa_\perp-\dot\varphi^2\tau^2)\left[\dot\varphi\tau-\frac{1}{2}(\kappa_\parallel-\kappa_\perp)\sin2\varphi\right]}{(\omega^2\tau^2-\kappa_\parallel\kappa_\perp-\dot\varphi^2\tau^2)^2+(\kappa_\parallel+\kappa_\perp)^2\omega^2\tau^2}. \tag{6}$$

For a sphere or a vertical cylinder one has $f_\parallel=f_\perp=f$ with $f=1/3$ and $f=1/2$, respectively. Thus, in terms of the magnetic permeability $\mu=1+4\pi\chi$, Eq. (4) gives $\kappa_\parallel=\kappa_\perp=\kappa$ with $\kappa=(\mu+2)/3$ for a spherical cavity and $\kappa=(\mu+1)/2$ for a cylindric one. Then, retaining in Eq. (6) only terms with the lowest power of the dimensionless angular displacement rate $\dot\varphi\tau$, we find the magnetic torque acting upon the sphere (index s) and the vertical cylinder (index c):

$$\bar{\mathcal{T}}_s=-\frac{9\chi\mathcal{H}_0^2V[(\mu+2)^2-9\omega^2\tau^2]}{2[(\mu+2)^2+9\omega^2\tau^2]^2}\dot\varphi\tau,$$

$$\bar{\mathcal{T}}_c=-\frac{2\chi\mathcal{H}_0^2V[(\mu+1)^2-4\omega^2\tau^2]}{[(\mu+1)^2+4\omega^2\tau^2]^2}\dot\varphi\tau. \tag{7}$$

Remarkably, the torques change sign at a certain critical value of the field frequency:

$$\omega_s\tau=(\mu+2)/3,\quad \omega_c\tau=(\mu+1)/2. \tag{8}$$

As long as $\omega\tau$ stays below this value, the magnetic torque is

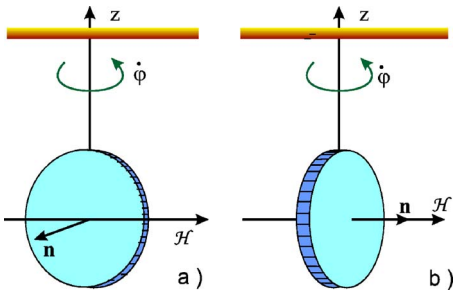

FIG. 1. (Color online) Equilibrium orientation of a disk-shaped ferrofluid pendulum with respect to oscillating magnetic field of low (a) and high (b) frequency.

directed opposite to the angular velocity, i.e., it plays the *restoring* role. However, as soon as the pumping frequency exceeds the threshold (8), the torque turns positive and tends to lead the pendulum away from equilibrium.

For a thin disk-shaped cell one can assume with a reasonable accuracy $f_\parallel=1$, $f_\perp=0$, so that $\kappa_\parallel=\mu$, $\kappa_\perp=1$ and hence the torque (6) takes the form

$$\bar{T}=\tfrac{1}{2}\chi\mathcal{H}_0^2V\frac{(\omega^2\tau^2-\mu-\dot{\varphi}^2\tau^2)(\dot{\varphi}\tau-2\pi\chi\sin 2\varphi)}{(\omega^2\tau^2-\mu-\dot{\varphi}^2\tau^2)^2+(\mu+1)^2\omega^2\tau^2}. \quad (9)$$

The main difference between Eqs. (7) and (9) is in the fact that axisymmetric cavities experience the magnetic torque only in motion, whereas the nonaxisymmetric cell is acted by the torque even in the state of rest: at $\dot{\varphi}=0$ Eq. (9) reduces to

$$\bar{T}=\frac{\chi\mathcal{H}_0^2V(\mu-1)(\mu-\omega^2\tau^2)}{4(\mu^2+\omega^2\tau^2)(1+\omega^2\tau^2)}\sin 2\varphi. \quad (10)$$

The equation of motion of the disk-shaped pendulum reads

$$\ddot{\varphi}+\Gamma\dot{\varphi}=\bar{T}/I, \quad (11)$$

where Γ is the friction coefficient and $I=\rho VR^2/4$ is the moment of inertia of a disk which rotates around its diameter. In the slowly oscillating magnetic field $\omega\tau<\sqrt{\mu}$, the equation describes small damped oscillations of the pendulum in the vicinity of the equilibrium position $\varphi=\pi/2$ [see Fig. 1(a)]: putting $\varphi=\pi/2+\varepsilon$, where $\varepsilon\ll 1$, one has

$$\ddot{\varepsilon}+\Gamma\dot{\varepsilon}+\omega_0^2\varepsilon=0,$$

$$\omega_0^2=\frac{\mathcal{H}_0^2(\mu-1)^2(\mu-\omega^2\tau^2)}{2\pi\rho R^2(\mu^2+\omega^2\tau^2)(1+\omega^2\tau^2)}. \quad (12)$$

Replacing here $\mathcal{H}_0^2/2$ by $\mathcal{H}^2$ one finds the pendulum eigenfrequency in a stationary field ($\omega=0$):

$$\omega_0=\frac{(\mu-1)\mathcal{H}}{R\sqrt{\pi\rho\mu}}.$$

At $\omega\tau=\sqrt{\mu}$ the pendulum changes the orientation of its state of rest. For a high enough pumping frequency $\omega\tau>\sqrt{\mu}$ and sufficiently low amplitudes of magnetic field (see below), it performs small damped oscillations around the equilibrium position $\varphi=0$ shown in Fig. 1(b):

$$\ddot{\varphi}+\Gamma\dot{\varphi}+\omega_0^2\varphi=0,$$

$$\omega_0^2=\frac{\mathcal{H}_0^2(\mu-1)^2(\omega^2\tau^2-\mu)}{2\pi\rho R^2(\mu^2+\omega^2\tau^2)(1+\omega^2\tau^2)}. \quad (13)$$

To explain the change of the equilibrium orientation in the field $\mathcal{H}_x=\mathcal{H}_0\cos\omega t$, we calculate the magnetic field energy $E(t)$ and the energy dissipation rate $Q(t)$. Within the approximation of the linear magnetization law $\mathbf{M}=\chi\mathbf{H}$, these values are given by

$$E(t)=-\tfrac{1}{2}(\boldsymbol{\mathcal{M}}\cdot\boldsymbol{\mathcal{H}})=-\tfrac{1}{2}VM_x\mathcal{H}_0\cos\omega t,$$

$$Q(t)=-(\boldsymbol{\mathcal{M}}\cdot\dot{\boldsymbol{\mathcal{H}}})=\omega VM_x\mathcal{H}_0\sin\omega t. \quad (14)$$

In the state of rest ($\dot{\varphi}=0$), Eqs. (5) prescribe the value of the in-axis component of the fluid magnetization

$$M_x=\chi\mathcal{H}_0\sin\omega\tau\left(\frac{\omega\tau\cos^2\varphi}{\mu^2+\omega^2\tau^2}+\frac{\omega\tau\sin^2\varphi}{1+\omega^2\tau^2}\right)$$

$$+\chi\mathcal{H}_0\cos\omega\tau\left(\frac{\mu\cos^2\varphi}{\mu^2+\omega^2\tau^2}+\frac{\sin^2\varphi}{1+\omega^2\tau^2}\right).$$

Substituting this into Eqs. (14) and averaging the relationships over the period of field variation yield

$$\bar{E}=-\frac{\chi\mathcal{H}_0^2V}{4}\left(\frac{\mu\cos^2\varphi}{\mu^2+\omega^2\tau^2}+\frac{\sin^2\varphi}{1+\omega^2\tau^2}\right), \quad (15)$$

$$\bar{Q}=\frac{\chi\mathcal{H}_0^2V}{2\tau}\omega^2\tau^2\left(\frac{\cos^2\varphi}{\mu^2+\omega^2\tau^2}+\frac{\sin^2\varphi}{1+\omega^2\tau^2}\right). \quad (16)$$

The equilibrium orientation of the cell with respect to the field direction corresponds to the minimum of magnetic energy at the low field frequencies $\omega\tau<\sqrt{\mu}$ and to the minimum of the energy dissipation at the high frequencies $\omega\tau>\sqrt{\mu}$. Indeed, in the limit of low frequencies the dissipation rate is negligible, while in the opposite limiting case one can neglect the energy. In the former case $\omega\tau<\sqrt{\mu}$, the energy $\bar{E}$ has a minimum at $\varphi=\pi/2$: magnetic field is almost non-perturbed when it flows down a thin disk [see Fig. 1(a)]. On the other hand, the rate of energy dissipation $\bar{Q}$ has the minimum at $\varphi=0$ at all frequencies. In fact, this is none other than the heat producing per time unit due to the ferrofluid re-magnetization. As seen from Eq. (16), the minimum of the heat production is reached when the cell is held perpendicularly to the field [Fig. 1(b)]: in this position the demagnetization factor $f_\parallel$ along the field direction equals unity, so that M_x takes its minimum value and hence $\bar{Q}$ is also minimal. Therefore, in accordance with the Le Chatelier principle, at high pumping frequencies the coin-shaped cell exposes to the field its head (tail).

III. LINEAR STABILITY OF EQUILIBRIUM STATES

Consider now the general case of arbitrary field amplitudes, pendulum angular displacements and angular velocities. Substituting the magnetic torque (9) into Eq. (11) leads to the dimensionless equation of motion

$$\ddot{\varphi} + 2\left[\alpha - \frac{\beta(\gamma^2 - \mu - \dot{\varphi}^2)}{(\gamma^2 - \mu - \dot{\varphi}^2)^2 + (\mu+1)^2\gamma^2}\right]\dot{\varphi} + \frac{\beta(\mu-1)(\gamma^2 - \mu - \dot{\varphi}^2)}{(\gamma^2 - \mu - \dot{\varphi}^2)^2 + (\mu+1)^2\gamma^2}\sin 2\varphi = 0, \quad (17)$$

where τ is chosen as a unit of time, and the new dimensionless parameters are

$$\gamma = \omega\tau, \quad \alpha = \tfrac{1}{2}\Gamma\tau, \quad \beta = \frac{\chi\mathcal{H}_0^2\tau^2}{\rho R^2}. \quad (18)$$

Equilibrium solutions of Eq. (17) correspond to $\varphi_0 = n\pi/2$, $n = 0, \pm 1, \pm 2, \ldots$: the container is at rest when either of its horizontal axes is parallel to the field. Invariance of Eq. (17) with respect to the transformation $\varphi \to \varphi + \pi$ allows to restrict the phase space of Eq. (17) to the cylinder $-\pi \le \varphi \le \pi$. Besides, there is a mirror-like symmetry with respect to the change of sign of φ.

Linearization near the equilibria yields the characteristic equation for the increment of perturbations λ:

$$\lambda^2 - 2\lambda\left(\frac{\beta(\gamma^2-\mu)}{(\gamma^2+\mu^2)(\gamma^2+1)} - \alpha\right) + (-1)^n\frac{2\beta(\mu-1)(\gamma^2-\mu)}{(\gamma^2+\mu^2)(\gamma^2+1)} = 0. \quad (19)$$

A mere look at this equation discloses the fact, already known from the previous section: the range of driving frequencies is divided in two parts. The case of low frequency $\gamma < \sqrt{\mu}$ [17] is relatively poor from the point of view of dynamics. Here, the last term in Eq. (19) is negative for even n and positive otherwise. Accordingly, the equilibrium with $\varphi = 0$ is always a saddle point. In contrast, the equilibria at $\varphi = \pm\pi/2$ are stable irrespective of the (of course, positive) value of β.

At the critical value $\gamma = \sqrt{\mu}$ a degenerate bifurcation occurs: every value of φ delivers a stationary solution of Eq. (17), so that a continuum of marginally stable fixed points arises. A breakup of this continuum in the direction of higher frequencies $\gamma > \sqrt{\mu}$ interchanges the stability properties of the equilibria. Under these frequency values, the states of rest at $\varphi = \pm\pi/2$ are saddles. The equilibrium at $\varphi = 0$, depending on the value of β, is either a node or a focus. The latter case corresponds to the range of β between the values β_-^{foc} and β_+^{foc}, where

$$\beta_\pm^{\text{foc}} = N\left[\mu + \alpha - 1 \pm \sqrt{(\mu+\alpha-1)^2 - \alpha^2}\right] \quad \text{with } N \equiv (\gamma^2+\mu^2)(\gamma^2+1)(\gamma^2-\mu)^{-1}. \quad (20)$$

In a realistic physical setup with fast modulation of the field and weak friction, the value of α is rather small. Accordingly, $\beta_-^{\text{foc}} \approx \alpha^2 N/(2\mu - 2)$ is also very small, whereas $\beta_+^{\text{foc}} \approx 2N(\mu - 1)$ is reasonably large. For very low or very high values of β the steady state at $\varphi = 0$ is a node. With the increase of β, evolution of the local phase portrait near this state follows the transformation of the equilibrium in the conventional Rayleigh (or Van der Pol) equation under the parameter variation: stable node → stable focus → unstable focus → unstable node.

Destabilization of equilibrium at $\varphi = 0$ occurs when the coefficient at $\dot{\varphi}$ (the "local friction") in Eq. (17) vanishes; this corresponds to the Hopf bifurcation which happens at

$$\beta = \beta_{\text{cr}} = \alpha\frac{(\gamma^2+\mu^2)(\gamma^2+1)}{\gamma^2-\mu}. \quad (21)$$

Substituting this into the last term of Eq. (17) determines the dimensionless eigenfrequency $\nu = \omega_0\tau$ of the pendulum critical oscillations

$$\nu_{\text{cr}} = \sqrt{2\alpha(\mu-1)}. \quad (22)$$

IV. WEAKLY NONLINEAR THEORY: ONSET OF OSCILLATIONS

Near $\beta = \beta_{\text{cr}}$, introduction of the complex variable

$$w = \frac{4\alpha(\mu-1)\varphi + 2\alpha(1-\beta/\beta_{\text{cr}})\dot{\varphi}}{\sqrt{8\alpha(\mu-1) - 4\alpha^2(1-\beta/\beta_{\text{cr}})^2}} - i\dot{\varphi} + \text{appropriate nonlinear terms} \quad (23)$$

turns Eq. (17) into

$$\dot{w} = \left(\alpha\frac{\beta-\beta_{\text{cr}}}{\beta_{\text{cr}}} - i\nu_{\text{cr}} + K|w|^2 + O(|w|^4)\right)w, \quad (24)$$

where the branching coefficient K is given by the expression

$$K = \frac{3\alpha[(\gamma^2-\mu)^2 - (\mu+1)^2\gamma^2]}{4(1+\gamma^2)(\gamma^2+\mu^2)(\gamma^2-\mu)}. \quad (25)$$

As shown above, oscillations arise at $\gamma > \sqrt{\mu}$. Therefore, along the neutral curve $\beta_{\text{cr}}(\gamma)$ the sign of K is governed by the numerator of Eq. (25). The latter changes its sign at $\gamma_* = (\mu + 1 + \sqrt{\mu^2 + 6\mu + 1})/2$. For $\gamma < \gamma_*$ the value of K is negative, thus the Hopf bifurcation is supercritical and creates the stable limit cycle. On the opposite, in the whole range of high driving frequencies $\gamma > \gamma_*$, the Hopf bifurcation is subcritical. As usual, the subcritical character of the bifurcation indicates a hysteresis and implies that oscillations are born with finite amplitude at a certain value of β below β_{cr}.

Close to the Hopf bifurcation, the amplitude of newborn oscillations approximately equals

$$w \approx \sqrt{\frac{\alpha(\beta-\beta_{\text{cr}})}{K\beta_{\text{cr}}}}. \quad (26)$$

In the region where K changes the sign (and, in fact, in a wide range around γ_*), the denominator of Eq. (26) is small. Therefore, the amplitude w as a function of β exhibits a rapid growth, so that already at small deviations of β from β_{cr} the diameter of the limit cycle in the phase space becomes comparable with the size of the cylinder: extrema of the angle φ approach the unstable equilibria at $\varphi = \pm\pi/2$.

In order to understand the transformations of the phase portrait of Eq. (17) far from the threshold of the linear stability β_{cr}, the local expansion (24) is insufficient. Indeed, as we will see below, the higher-order nonlinear effects occur

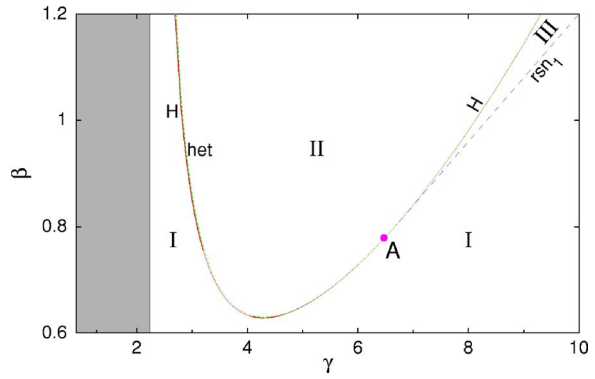

FIG. 2. (Color online) Diagram of states for Eq. (17) with $\alpha=0.01$, $\mu=5$. Gray stripe: stable equilibria at $\varphi=\pm\pi/2$, I: stable equilibrium at $\varphi=0$, II: stable rotations of the cell, III: hysteresis between equilibrium and rotations. *H*: Hopf bifurcation of the equilibrium, het: formation of heteroclinic contour between the saddles, rsn_1: finite-amplitude birth of rotations. Filled circle *A*: change of character of the Hopf bifurcation at γ_*.

already reasonably close to the destabilization of the equilibrium. Further analysis requires a combination of qualitative reasoning with numerical computations.

V. STRONG NONLINEARITIES: BIFURCATION DIAGRAMS

Global evolution of nonstationary regimes is related to creation of heteroclinic contours formed by separatrices which connect the equilibria at $\varphi=\pm\pi/2$. Due to the mentioned smallness of $|K|$, this event occurs rather close to the Hopf bifurcation: on the state diagram presented in Fig. 2, the curve *H* of the Hopf bifurcation and the curve het of the heteroclinic bifurcation are almost indistinguishable. These curves intersect near γ_* (but not exactly at γ_*: see the detailed explanation and the plots below). For minor values of γ the curve *H* lies slightly below; for higher values of γ the curve het is the lower of the two. An additional bifurcational curve rsn_1 is located to the right of γ_* and below *H*; it marks the saddle-node bifurcation: finite-amplitude birth of periodic solutions [19] corresponding to rotations of container around its axis. In the wedge-shaped domain between rsn_1 and *H* a hysteresis is observed: here, regime of stable rotations (in fact, two such regimes: the clockwise one and the counterclockwise one) coexists with the stable equilibrium.

At the first look, the events—at least for $\gamma<\gamma_*$—are analogous to the textbook transformation "oscillation → rotation" in the cylindric phase space of a pendulum governed by $\ddot{\varphi}+\sin\varphi=0$. It may seem that through the mediation of heteroclinic orbits stable oscillations near the state of rest are replaced by rotation of the container around its vertical axis.

Unfortunately, this simplistic bifurcation scenario is incompatible with the dynamical system (17). Incompatibility follows from the fact that the coefficient at λ in Eq. (19), i.e., the sum of the roots of this quadratic equation, is independent from *n*: the same for the state of rest at $\varphi=0$ and for the equilibria at $\varphi=\pm\pi/2$. Accordingly, the sum of two real increments for perturbations near symmetric saddle points at $\varphi=\pm\pi/2$ is negative for $\beta<\beta_{\mathrm{cr}}$ and positive for $\beta>\beta_{\mathrm{cr}}$. The sign of this sum of eigenvalues ("saddle index"), in its turn, is crucial for the stability of periodic solutions born from the breakup of the homoclinic or heteroclinic orbits (see, e.g., Ref. [18]). If the sum is positive, expansion in the flow near the saddle prevails over contraction, hence the branching periodic solution is unstable. If the sum is negative, contraction dominates and the bifurcating periodic state is attracting. The consequence: if heteroclinic contour is present at a certain value of β above the Hopf bifurcation, it is repelling and, hence, cannot serve as a switching mediator between stable oscillations and stable rotation. Similarly, if such contour is formed below the Hopf bifurcation, it is attracting, and therefore cannot match unstable oscillations with unstable rotation.

The actual bifurcation diagram on the parameter plane γ, β is a bit more complicated. Its organizing centers are two codimension-2 points: the point *A* on the curve *H* of the Hopf bifurcation in which the branching coefficient *K* changes sign, and the "neutral heteroclinic contour:" the point *B* on the curve het in which the sum of roots of Eq. (19) vanishes (due to the mentioned *n* independence of the corresponding coefficient, exactly at this point the curve het crosses the curve of the Hopf bifurcation). The abscissa value γ_B of the point *B* slightly exceeds the abscissa value γ_* of the point *A*. Along with the curves *H* and het, the diagram includes five different curves which correspond to saddle-node bifurcations for periodic solutions of Eq. (17). In the course of these saddle-node bifurcations, stable limit cycles (oscillations or rotations) coalesce with the unstable ones and disappear.

The neighborhood of both codimension-two points is shown in Fig. 3. Since nearly all transitions occur in the extremely narrow interval of the values of β, we have chosen in Fig. 3(a) as the vertical coordinate not the value of β itself, but its deviation β-β_{het} from the value which corresponds to the formation of the heteroclinic contour. Even in these coordinates, important details of location of certain curves can hardly be resolved, therefore we supply also the schematic presentation of the bifurcation diagram in Fig. 3(b).

Intersections of bifurcation curves divide the parameter plane into ten regions of qualitatively different dynamics; in Fig. 3(b) they are labeled in the clockwise order. Figure 4 presents qualitative phase portraits for each of the regions; solid curves denote stable states, the dashed lines show the unstable ones, whereas the dotted curves depict transients with "typical" initial conditions.

Of ten segments of the bifurcation diagram, only three are "macroscopically" resolvable in the basic state diagram of Fig. 2: the regions 1, 5, and 10 (they correspond, respectively, to regions I, II, and III in Fig. 2). However, without the remaining minor regions the bifurcation diagram would be inconsistent.

Let us proceed to the brief description of the typical bifurcation scenarios. The point *B* of the "neutral heteroclinic contour" is an important landmark: to the left from *B* the contour on the line het is repelling and mediates between the unstable states (oscillation and rotations). In contrast, to the right from *B* the heteroclinic contour is attracting, therefore

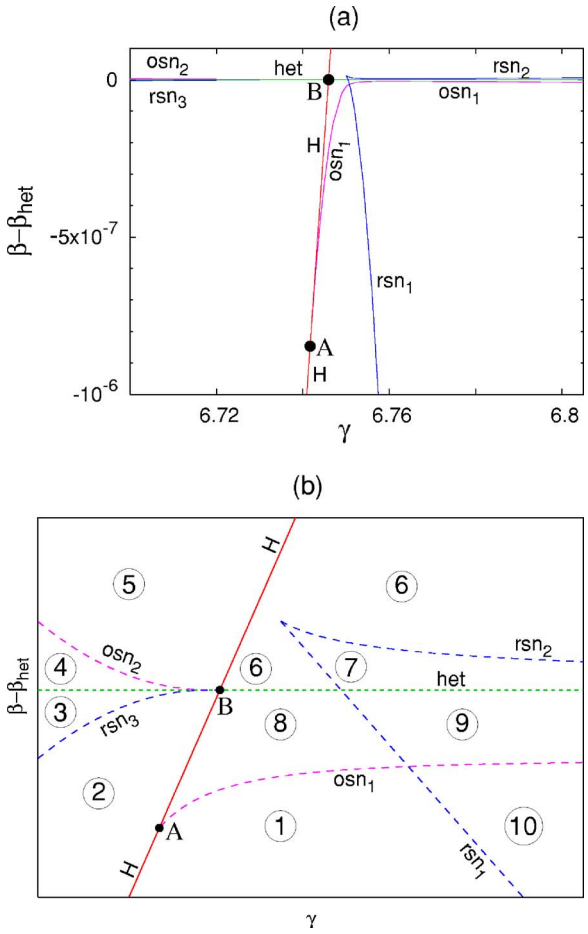

FIG. 3. (Color online) Bifurcation diagram for Eq. (17) with $\alpha=0.01$, $\mu=5$. (a) Computed diagram, (b) schematic diagram. H: Hopf bifurcation of the equilibrium, het: formation of heteroclinic contour, $\mathrm{osn}_{1,2,3}$: saddle-node bifurcations for oscillations, $\mathrm{rsn}_{1,2,3}$: saddle-node bifurcations for rotational states. Filled circles A,B: bifurcations of codimension 2.

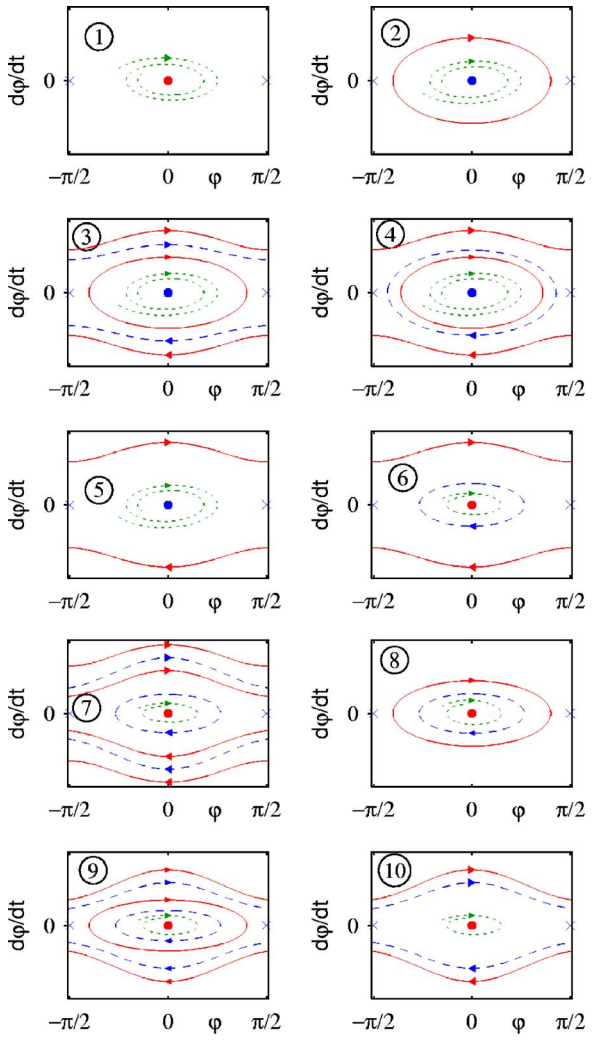

FIG. 4. (Color online) Qualitative phase portraits for Eq. (17) with $\alpha=0.01$, $\mu=5$, variable γ and β. Numbers on subplots correspond to numbers of regions in Fig. 3(b). Filled circles: equilibrium at $\varphi=0$. Crosses: saddle points at $\varphi=\pm\pi/2$. Solid (red) curves: stable periodic states. Dashed (blue) curves: unstable periodic states. Dotted (green) curves: transients.

with its help stable oscillations are transformed into stable rotation. The point B is an origin of two further bifurcation curves, both of them corresponding to saddle-node lines bifurcations: the line rsn_1 below het on which a stable and an unstable rotation solutions are born, and a line osn_1 above het on which the stable and the unstable oscillatory states collide and disappear. These curves, located to the left from the point B, delineate the exponentially thin wedge of hysteresis: as γ tends to γ_B, the distance between rsn_1 and rsn_2 decays as $(\gamma_B-\gamma)e^{-\epsilon/(\gamma_B-\gamma)}$ with positive ϵ.

Accordingly, for $\gamma<\gamma_*$ the increase of β results in the following bifurcation sequence.

(Region 1) Below the curve H the only attracting regime is the equilibrium state.

(Regions $1\rightarrow2$) On the curve H the supercritical Hopf bifurcation takes place; between H and the curve rsn_3 the oscillating solution is globally attracting.

(Regions $2\rightarrow3$) On the curve rsn_3 two (the clockwise one and the counterclockwise one) stable rotational states are born with finite amplitude; above the curve each of these neutrally stable solutions disintegrates into a stable one and an unstable one. Since the oscillating state is stable as well, in this parameter region a hysteresis is observed. Further growth of β leads to the decrease of the amplitude of the unstable rotational state.

(Regions $3\rightarrow4$) On the curve het the unstable rotational solutions touch "from the outside" the separatrices of the saddle equilibria at $\varphi=\pm\pi/2$ and form the heteroclinic contour which encircles the cylinder. After the breakup of this contour under the increase of β, unstable rotations are replaced by the unstable oscillatory state. The closed solution curve corresponding to this state separates in the phase space the attraction domains of the stable rotations and stable oscillations.

(Regions $4\rightarrow5$) On the curve osn_1 the limit cycles of stable and unstable oscillations collide and disappear. The remaining rotational state becomes the global attractor.

To the right of the point A (that is, for $\gamma>\gamma_*$) the bifurcation scenarios are different. On the curve osn_1 which terminates in this point, a saddle-node bifurcation for oscilla-

tory states takes place: here the oscillations are born with finite amplitude. In addition, this domain contains curves rsn_2 and rsn_3 on which the saddle-node bifurcations of rotational states occur. Note an additional codimension-two point where the latter curves join in a singularity of the cusp type.

In this part of the diagram, various bifurcation sequences are possible; we explain below only the "most relevant" one (it remains valid also for high values of γ).

(Region 1) Below all bifurcation curves, the only attracting regime is the state of rest.

(Regions $1 \rightarrow 10$) On the curve rsn_1 the limit cycles corresponding to rotational states are born in a saddle-node bifurcation. As a result, in region 10 the stable equilibrium coexists with two (clockwise and counterclockwise) rotations.

(Regions $10 \rightarrow 9$) On the curve osn_2 the saddle-node bifurcation gives birth to the limit cycle which correspond to oscillations. Therefore, in region 9, there is a triple hysteresis: depending on initial conditions, one can observe the stable equilibrium, the stable oscillations and the stable rotations. The phase curves of unstable oscillations and unstable rotations serve as boundaries of the basins of attractions of these regimes.

(Regions $9 \rightarrow 7$) With the growth of β the amplitude of the stable oscillations increases. On approaching the curve het the corresponding limit cycle touches "from inside" the separatrices of the saddle-points at $\varphi = \pm \pi/2$: the heteroclinic contour appears. Its subsequent breakup leaves in the phase space two new stable invariant curves which encompass the entire cylinder; they, of course, correspond to stable rotations. Thereby, in region 7 for each direction there are *two* coexisting stable rotational modes: the slower one (born from the heteroclinic bifurcation) and the faster one. Notably, the state of rest is stable as well.

(Regions $7 \rightarrow 6$) The invariant curve corresponding to slow stable rotations approaches from inside the curves of unstable rotations. On the line rsn_2 these regimes collide and disappear. In region 6 there is a hysteresis between the stable equilibrium and stable rotations; their domains of attraction are separated by the phase curve of unstable oscillations.

(Regions $6 \rightarrow 5$) On approaching the curve H of the Hopf bifurcation (which is subcritical in this part of the diagram) the size of the unstable limit cycle decreases. On the curve H this cycle shrinks into the point; the only attracting state in region 5 is the rotation, either clockwise or counterclockwise.

In the above descriptions we have not mentioned the region 8; in this curved quadrangular segment of the parameter plane, limited by four bifurcation curves, the stable equilibrium coexists with the stable oscillations. Smallness of this region makes it a difficult object for an experimental observation.

Summarizing the bifurcation diagrams, the increase of the field intensity β invariably transforms the observable state from the stable equilibrium to the rotation of container around its axis. However, the intermediate stages of this transformation depend on the value of the pumping frequency γ (and, partially, on the initial conditions of the experiment).

VI. DISCUSSION

We have shown that the state of rest and the dynamical behavior of a disklike ferrofluidic pendulum in an alternate magnetic field depend on the dimensionless field amplitude β and frequency γ. In a stationary or low-oscillating field ($\gamma < \sqrt{\mu}$), the pendulum is at rest for arbitrary values of β, exposing to the field its edge. For $\gamma > \sqrt{\mu}$ and the weak field, $\beta < \beta_{\mathrm{cr}}$, the disk is at rest as well but changes its orientation: now it exposes to the field its broad side. This abrupt 90° turn of the equilibrium configuration, occurring at the field frequency $\omega = \sqrt{\mu}/\tau$ can be used for an efficient experimental measurement of τ.

Further, in the sufficiently strong alternate field, the state of rest is replaced by oscillations near the equilibrium. The oscillations, in their turn, yield to rotations of the disk-shaped container around its vertical axis. Scenarios of transition from oscillations to rotations are centered on a heteroclinic bifurcation and include also several saddle-node bifurcations of periodic states.

Let us evaluate the strength and frequency of the driving magnetic field which are required in order to observe these effects in an experiment. According to Eq. (18), the critical amplitude of the field is expressed through the function $\beta_{\mathrm{cr}}(\gamma)$ given by Eq. (21). This function has a minimum $\beta_{\mathrm{cr}}^{\min}$ at $\gamma = \gamma_m$:

$$\gamma_m^2 = \mu + (\mu + 1)\sqrt{\mu}, \quad \beta_{\mathrm{cr}}^{\min} = (\mu + 1)(\sqrt{\mu} + 1)^2. \quad (27)$$

Substituting this into the definition of β [see Eq. (18)] delivers the minimal value of the necessary field amplitude. Its square is

$$(\mathcal{H}_0^{\min})^2 = \frac{2\pi\rho R^2 \Gamma(\mu + 1)(\sqrt{\mu} + 1)^2}{(\mu - 1)\tau}. \quad (28)$$

In addition to the parameters of the ferrofluid and the radius of the cell, Eq. (28) contains an ill-defined parameter of

the experimental setup—the friction coefficient Γ. To estimate it, recall that we neglect here the elasticity of the fiber on which the container is suspended. In other words, the eigenfrequency ω_0^{el} of torsional oscillations caused by the elasticity should be much lower than the frequency of oscillations ω_0 enforced by the field. But the lower the eigenfrequency, the smaller is the quality factor $q = \omega_0^{\mathrm{el}}/\Gamma$. Then, assuming the rather long period of pendulum oscillations $T_{\mathrm{el}} = 5$ s and the reasonably low quality factor $q = 5$, we arrive at $\Gamma = 2\pi/(qT_{\mathrm{el}}) \approx 0.25\ \mathrm{s}^{-1}$.

Take the hollow flat disk of $R = 13$ mm—similar to inch-wide coins widespread in many countries—filled with the same glycerine-based cobalt ferrite ferrofluid as was used in the experiments of Gazeau *et al.* [13]. The relaxation magnetization time of the fluid was $\tau = 8 \times 10^{-3}$ s; this yields an estimate $\alpha = \Gamma\tau/2 = 10^{-3}$. Other parameters of the fluid were the volume fraction of magnetic grains $\phi = 13\%$, the density $\rho = 1.85\ \mathrm{g/cm^3}$, $\mu = 5.4$, $\eta = 50$ Ps. Substituting those values and the above estimate for Γ into expressions (27) and (28) provides the amplitude and frequency of the critical (minimal) field

$$\mathcal{H}_0^{\min} = 99.3 \text{ Oe}, \quad \omega_m/(2\pi) = \gamma_m/(2\pi\tau) = 89.6 \text{ Hz}.$$

Checking self-consistency, we observe that the squared dimensionless eigenfrequency $\nu_{\rm el}=\omega_0^{\rm el}\tau$ of oscillations caused by the elasticity of the fiber is much lower than the squared eigenfrequency (22) of the field-induced critical oscillations

$$\left(\frac{\nu_{\rm el}}{\nu_{\rm cr}}\right)^2 = \frac{2\pi^2\tau^2}{\alpha(\mu-1)T_{\rm el}^2} \approx 1.15\times 10^{-2}. \tag{29}$$

Analysis which we have performed in the preceding sections, has been based on two restrictive assumptions. First, we treated only the situation in which the frequency of the field by far exceeds the eigenfrequency of the pendulum. Accordingly, our results refer to the observables averaged over the period of the field. If two frequencies are of the same order, the averaged quantities should be replaced by instantaneous values. Instead of the autonomous second-order differential Eq. (17), the nonautonomous system of the fourth order should be treated: Eqs (3)+equation of the second order for the angular variable. Therefore, instead of the steady states, periodic regimes will be observed: the disk varies in time its position, closely following with its appropriate (edge or head, respectively) side the instantaneous direction of the alternate field. Further, periodic attractors (oscillations, rotations) of the averaged equation will be replaced by quasiperiodic oscillations/rotations. If the two frequencies are close to resonance ratios, more complicated dynamics can be expected (see Ref. [16]).

Another important assumption in the above analysis has been the neglect of the elasticity of the fiber on which the pendulum is suspended—see Eq. (29). Taking weak elasticity into account would single out the orientation $\varphi_{\rm nt}$ to the non-twisted fiber and add to the right-hand side of Eq. (17) a term, proportional to $\varphi-\varphi_{\rm nt}$. The topological implications of this term are far-reaching: the cylindrical phase place should be replaced by the phase plane; the equilibria slightly deviate from $\varphi=n\pi/2$ at small $|n|$ and completely disappear for sufficiently large $|n|$. The degeneracy of the abrupt nonhysteretic transition between two states of rest at $\gamma=\sqrt{\mu}$ is lifted; instead, a narrow interval of the values of γ emerges, in which the stable equilibrium of the pendulum rapidly (but continuously) changes its orientation. The above interpretation of this transition in terms of balance of energy should in this case be complemented by incorporation of the elastic energy. Further, since the "almost head" and "almost tail" orientation of the coin-shaped pendulum are no more equivalent, they experience the Hopf bifurcation at slightly different values of β. The rotating states are, of course, impossible; they are replaced by "large-scale" (involving many complete revolutions of the disk around the axis) oscillations. Finally, the formation of the heteroclinic contour disintegrates into a sequence of homoclinic and saddle-node bifurcations. All these qualitative changes, however, remain almost invisible for an observer as long as the elasticity of the fiber is sufficiently small.

ACKNOWLEDGMENTS

The work of M. S. was supported by the Israeli Science Foundation (Grant No. 272/03) and the U. S.–Israeli Binational Science Foundation (Grant No. 2004081). M. Z. acknowledges the support from SFB-555 of the Deutsche Forschungsgemeinschaft and is grateful for hospitality during his short research stay at the Ben-Gurion University.

[1] J. P. McTague, J. Chem. Phys. **51**, 133 (1969).
[2] M. I. Shliomis, Zh. Eksp. Teor. Fiz. **61**, 2411 (1971) [Sov. Phys. JETP **34**, 1291 (1972)]; , Usp. Fiz. Nauk **112**, 427 (1974) [Sov. Phys. Usp. **17**, 153 (1974)].
[3] M. A. Martsenyuk, Yu. L. Raikher, and M. I. Shliomis, Zh. Eksp. Teor. Fiz. **65**, 834 (1973) [Sov. Phys. JETP **38**, 413 (1974)].
[4] R. E. Rosensweig, *Ferrohydrodynamics* (Cambridge University, Cambridge, England, 1985).
[5] B. U. Felderhof, Phys. Rev. E **62**, 3848 (2000).
[6] M. I. Shliomis, Phys. Rev. E **64**, 063501 (2001); **64**, 060501(R) (2001).
[7] S. Odenbach, *Magnetoviscous Effects in Ferrofluids*, Vol. 71m of Lecture Notes in Physics (Springer, Berlin, 2002).
[8] R. Patel, R. V. Upadhyay, and R. V. Mehta, J. Colloid Interface Sci. **263**, 661 (2003).
[9] M. I. Shliomis, in *Ferrofluids. Magnetically Controllable Fluids and Their Applications*, edited by S. Odenbach, Vol. 594 of Lecture Notes in Physics (Springer, Berlin, 2002), pp. 85–111.
[10] M. I. Shliomis and K. I. Morozov, Phys. Fluids **6**, 2855 (1994).
[11] J.-C. Bacri, R. Perzynski, M. I. Shliomis, and G. I. Burde, Phys. Rev. Lett. **75**, 2128 (1995).
[12] R. E. Rosensweig, Science **271**, 614 (1996).
[13] F. Gazeau, C. Baravian, J.-C. Bacri, R. Perzynski, and M. I. Shliomis, Phys. Rev. E **56**, 614 (1997).
[14] A. Zeuner, R. Richter, and I. Rehberg, Phys. Rev. E **58**, 6287 (1998).
[15] A. P. Krekhov, M. I. Shliomis, and S. Kamiyama, Phys. Fluids **17**, 033105 (2005).
[16] M. I. Shliomis and M. A. Zaks, Phys. Rev. Lett. **93**, 047202 (2004).
[17] Recall that being less than $\sqrt{\mu}$ the dimensionless pumping frequency γ should be still high compared to the pendulum critical eigenfrequency $\nu_{\rm cr}\sim\sqrt{2\alpha\mu}$. These conditions, $\sqrt{\mu}>\gamma\gg\sqrt{2\alpha\mu}$, are satisfied owing to the smallness of the friction coefficient α.
[18] P. Glendinning, *Stability, Instability and Chaos: An Introduction to the Theory of Nonlinear Differential Equations* (Cambridge University Press, Cambridge, 1994).
[19] In terms of the angle φ unwrapped onto a phase plane, rotational states correspond to unbounded motions. Below, we use the vocabulary of the cylindrical phase space where such states are periodic in time and their phase curves are limit cycles. Of course, such limit cycles are topologically distinct from limit cycles corresponding to oscillations around the state of rest.